Protein aggregation drives cell aging in a size-specific manner in *Escherichia coli*

Linda Wagener[1], Arpita Nath[1], Murat Tuğrul[1], Abram Aertsen[2], Ulrich K. Steiner[1,†], Audrey M. Proenca[1,†]*

[1] Freie Universität Berlin, Institute of Biology, Berlin, Germany.

[2] KU Leuven, Department of Microbial and Molecular Systems, Leuven, Belgium

[†] These authors contributed equally to this work.

* correspondence: aproenca@zedat.fu-berlin.de

ABSTRACT

Aging, the decline in physiological function over time, is marked by the intracellular accumulation of damaged components. It can be attributed to a trade-off between the investment into organismal maintenance and the production of high-quality offspring, where the parent accumulates damage over time and retains it upon reproduction, while the offspring is rejuvenated. Asymmetric damage partitioning has been observed even in simple unicellular organisms, such as *Escherichia coli* cells that retain aggregates of misfolded proteins during cell division. However, recent studies presented conflicting evidence on the effect of protein aggregates on fitness, ranging from detrimental effects on cell growth to enhanced stress survival. Here, we show that the decisive factor driving growth decline in *E. coli* is not the presence of a protein aggregate, but the proportion of the intracellular space occupied by it. By following single-cell *E. coli* lineages expressing fluorescently labeled DnaK chaperones, we quantified damage accumulation and partitioning across generations in microfluidic devices. Our results suggest that the aggregation of damaged proteins allows cells to keep damage separate from vital processes and compensate for the lost intracellular space by growing to larger sizes, a process which results in morphologically asymmetrical divisions. In line with other recent evidence, this points to a more complex role of protein aggregation, with implications for our understanding of the cellular mechanisms underlying aging as well as its evolutionary origins.

INTRODUCTION

Organisms age due to a decline in fitness over time, losing physiological integrity and becoming increasingly more vulnerable to death (*1*, *2*). Aging can be attributed to a trade-off between reproduction and somatic repair, in which the maintenance of the germline comes at the cost of an increased damage accumulation by a "disposable" soma (*3*). Although unicellular organisms lack a differentiation between soma and germline, similar processes of asymmetric damage partitioning have led to the emergence of aging in yeast (*4*), algae (*5*), and bacteria (*6*, *7*). This is particularly relevant since single-cell organisms can provide a system where the progression of aging hallmarks can be observed and quantified *in vivo*, which represents a major challenge in the field (*1*).

Symmetrically dividing prokaryotes, such as the rod-shaped model bacterium *Escherichia coli*, were once considered not to exhibit the aging phenotype. However, despite splitting into two cells that are morphologically and genetically identical, *E. coli* displays a deterministic physiological asymmetry (*7*–*9*). Cells inheriting an old pole for multiple generations age, exhibiting slower growth rates, decreased offspring production, and increased mortality rates (*7*, *10*). In contrast, cells inheriting a new pole, which was synthesized during the previous fission event, rejuvenate. Because this asymmetry presumably arises through the uneven partitioning of intracellular damage (*8*, *11*, *12*), it can be regarded as akin to a soma-germline delineation (*13*), effectively creating a separation between an aging mother cell and a rejuvenated daughter with each division. Models on asymmetry in single-cell organisms underpin these findings by showing that asymmetrical segregation of damage is likely to evolve as a strategy to increase fitness in the face of high levels of cellular damage (*14*–*16*).

The accumulation of misfolded proteins is widely regarded as an age-associated source of intracellular damage. Sources of proteotoxic stress can cause proteins to change from their native conformation to a misfolded one, rendering them inactive or even toxic to the cell. The misfolding of a protein can expose its hydrophobic portions, leading it to bind to other proteins and thereby interfere with their functioning (*17*). This disruption of proteostasis can lead to the formation of insoluble protein aggregates within a cell. In mammals, the increased accumulation of misfolded proteins and decreased repair capacity is considered an aging hallmark (*1*), often leading to the development of aging-related diseases such as Parkinson's and Alzheimer's (*18*). In a striking parallel with eukaryotic processes, *E. coli* aging has been attributed to protein aggregation. Misfolded proteins, which can appear anywhere within the cell, tend to cluster together. If such aggregates become too large to diffuse through the nucleoid (*12*, *19*, *20*), they can become stuck at the cell pole as it is successively inherited across generations, thus being preferentially retained by the mother cell (*8*, *11*). Since the presence of aggregates hinders diffusion of other intracellular components (*19*), it might also cause the mother cell to inherit fewer ribosomes (*21*) and newly synthesized proteins (*22*). Daughter cells, in contrast, inherit a larger share of "good" components along with smaller damage loads, leading to improved rates of growth and gene expression (*23*).

Proteostasis is essential for cellular functioning, and protein repair is key for healthy cell growth. The protein repair machinery of bacteria deals with damage by degrading or refolding misfolded proteins, thereby preventing aggregation, or by disaggregating already formed aggregates (*24*). As such, protein aggregation mainly occurs when a cell accumulates damage at a faster rate than it can repair (*11*), at which point *E. coli* cells exhibit increasing amounts of polar aggregates. Computational analyses suggest that damage aggregation can be advantageous in face of stress, as it allows for the asymmetric partitioning of intracellular damage between aging mothers and rejuvenating daughters (*25*). If the same damage loads were to be symmetrically partitioned, the preservation of cellular functions would likely require a larger investment into repair activities.

While it is known that protein aggregates form in response to stress, their correlation with aging phenotypes has been questioned by recent studies. The observation of large aggregates in maternal old poles has been attributed to the choice of fluorescent marker in earlier research, which used the small chaperone IbpA labeled with yellow fluorescent protein (YFP) for damage quantification (*8*, *26*). When the reporter was exchanged for a monomeric superfolder green fluorescent protein (msfGFP), heat shock-induced aggregates had no negative impact on fitness (*27*). Similarly, *E. coli* lineages grown in unstressed conditions did not accumulate polar aggregates, despite consistently exhibiting a physiological asymmetry between mothers and daughters (*28*). Once the formation of aggregates is induced, however, they can have a protective effect against further heat shock (*27*) and promote antibiotic persistence (*29*), suggesting that their presence does not always imply a fitness decline.

The observation of an age-related loss of proteostasis in prokaryotes has framed this process as a conserved aging hallmark among cellular organisms (*30*). It is therefore imperative to elucidate the recent conflicting evidence on the correlation between protein aggregation and bacterial aging. To address this, we quantified the accumulation of intracellular damage using DnaK, a heat-shock protein that plays a central role in protein quality control, acting both to refold soluble misfolded proteins (*31*) and to disaggregate protein aggregates (*11*, *17*). As a damage marker, most previous studies have focused on the Inclusion Body Protein A (IbpA) (*8*, *12*, *27*), which co-localizes with misfolded proteins. DnaK, in contrast, reports not only the localization of damage, but also indicates that it is being actively repaired by the cell in an energy-consuming process (*11*, *32*). Quantifying the accumulation of DnaK-labeled damage, we found that protein aggregates accumulate in maternal old poles over generations, even as mother cells reach the state of long-term growth stability that is commonly observed within microfluidic devices (*9*, *28*, *33*). By itself, the presence of a polar aggregate did not lead to lower elongation rates. Instead, we found that the main determinant of aging is the relative size of the protein aggregate, compared to the total length of a cell. We found that aging also leads to an increase in maternal cell size, which buffers the effect of damage accumulation and allows the cell to maintain stable elongation rates despite harboring large clusters of misfolded proteins. We thus propose that protein aggregation is a hallmark of bacterial aging, driving a progressive functional decline in a size-dependent manner.

RESULTS

E. coli expressing DnaK-msfGFP shows wild-type levels of asymmetry

To evaluate whether protein misfolding and aggregation act as a driver of bacterial aging, we quantified damage accumulation at the single-cell level. For this, we used *E. coli* cells expressing DnaK-msfGFP as a reporter for both the subcellular localization of damaged components and the ongoing repair activity that is expected to be energy-costly (*11*). We ensured stable conditions by culturing cells in the mother machine microfluidic device (*33*), containing thousands of growth wells that receive a continuous supply of nutrients. The closed end of each well traps the cell inheriting an old pole with each division, which can be regarded as the mother cell. The opposite pole, synthesized during the previous fission, is considered a new pole that is inherited by the daughter cell. While the device traps mother cells for hundreds of generations, daughters are lost into the flow channel after a few divisions. Here, we followed populations over 48h, measuring growth physiology and damage accumulation in mother cells over time, and in daughter cells over their first cell cycle.

First, to determine whether the expression of the fluorescent reporter had an influence on cell growth, we compared the reporter strain to wild-type *E. coli* MG1655. Since our work explores the impact of protein aggregates on physiological asymmetry, we started by measuring growth asymmetry as the ratio between mother and daughter elongation rates (Fig. 1A). The DnaK-msfGFP strain had

lower divisional asymmetry (0.875 ± 0.192, mean ± SD; n = 18,756 division events) than the wild-type (0.858 ± 0.181; n = 15,247), suggesting that daughter cells had a slightly lower growth advantage over their mothers when expressing the fluorescent marker (Wilcoxon rank-sum test, W = 134,320,466, $p < 0.001$). A small growth difference could be observed in mean elongation rates of both strains, with DnaK-msfGFP cells exhibiting a 5.6% lower elongation rate (0.016 ± 0.005 min^{-1}) than the wild-type (0.017 ± 0.005 min^{-1}; Wilcoxon rank-sum test, W = 459,374,003, $p < 0.001$; Fig. 1BC).

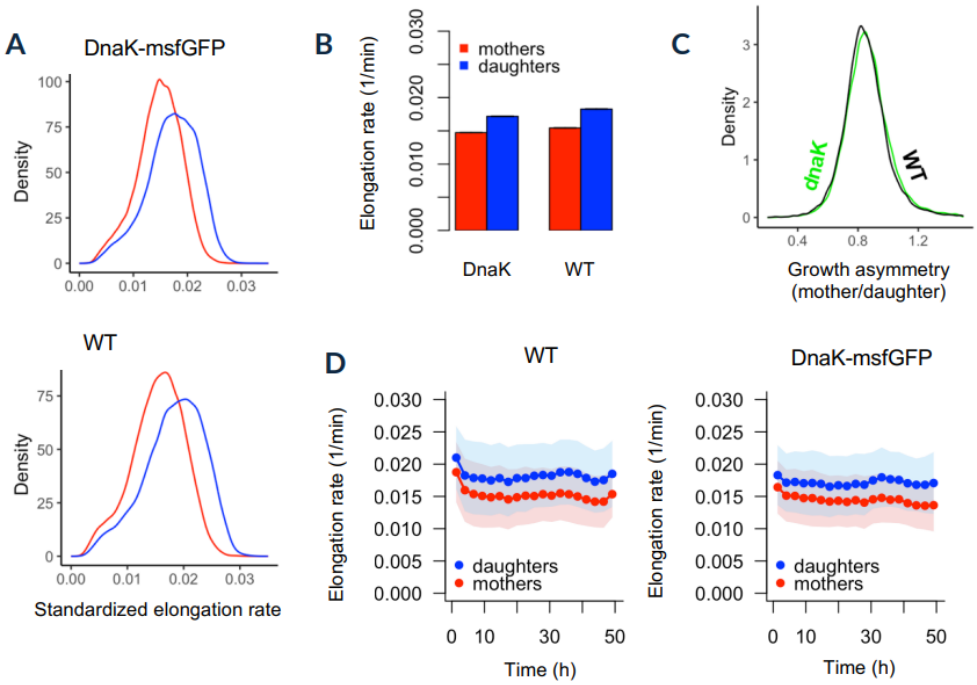

Fig. 1. Strains expressing DnaK-msfGFP show asymmetry equivalent to wild type bacteria. (A) Density plots showing growth as determined by elongation rates in *E. coli* strains MG1655 Δ*lacY dnaK-msfGFP* and MG1655 Δ*lacY* (WT). Red lines represent mother cells and blue lines represent daughter cells. Elongation rates were standardized to compare the growth asymmetry between the two strains. (B) Mean elongation rates in both strains, showing the asymmetry of growth between mother and daughter cells. Error bars = 95% confidence intervals. (C) Both strains showed similar growth asymmetry, as expressed by mother-daughter elongation rate ratios. (D) In both strains, mother and daughter cells showed stable growth over time, with mothers consistently growing more slowly than daughters. Bins = mean ± standard deviation.

The two strains showed small differences in elongation rates over time (Fig. 1D). Both exhibited a slight increase in growth asymmetry over time, since maternal elongation rates showed a small decrease while their daughters remained constant. We verified this through an analysis of covariance (ANCOVA), using elongation rates as the response variable and strain (DnaK-msfGFP / wild-type), inherited pole (mother / daughter) and time as explanatory variables. The best supported model included all three variables and their interactions, meaning that the protein fusion had an influence on growth (F-test, $F_{4, 64559} = 143.6$, $p < 0.001$, $R^2 = 0.09$). While the two strains showed these significant differences in growth and asymmetry, the small effect sizes suggest that these differences are of limited biological concern for the context of this work. We conclude that the DnaK-msfGFP is a suitable translational reporter for quantifying the correlations between protein aggregation, cell growth, and physiological asymmetry leading to bacterial aging.

Mean intracellular DnaK concentration increases with age

To determine whether aging correlates with the accumulation of misfolded proteins, whether soluble or aggregated, we measured mean fluorescence levels at the beginning of each generation. We

found that the levels of intracellular damage in mother cells increased over time, which was contrasted by no relevant increase in daughter cells (Fig. 2A). Through an ANCOVA, we verified that pole inheritance (mother/ daughter), time, and their interaction affected mean fluorescence (F test, $F_{3, 35991}$ =1209, $p < 0.001$, $R^2 = 0.09$). To determine whether the increase in DnaK concentration was due to protein aggregation, we estimated mean fluorescence levels of cells with and without visible aggregates (Fig. 2B). The resulting pattern was equivalent to that of mother-daughter fluorescence levels, suggesting that the increase in intracellular damage levels found in mother cells was due to the accumulation of protein aggregates, which might be mostly absent among daughter cells. Since DnaK acts to refold and disaggregate damaged proteins, consuming ATP in the process, this also suggests an asymmetric allocation of resources where mother cells show a greater investment into repair activities.

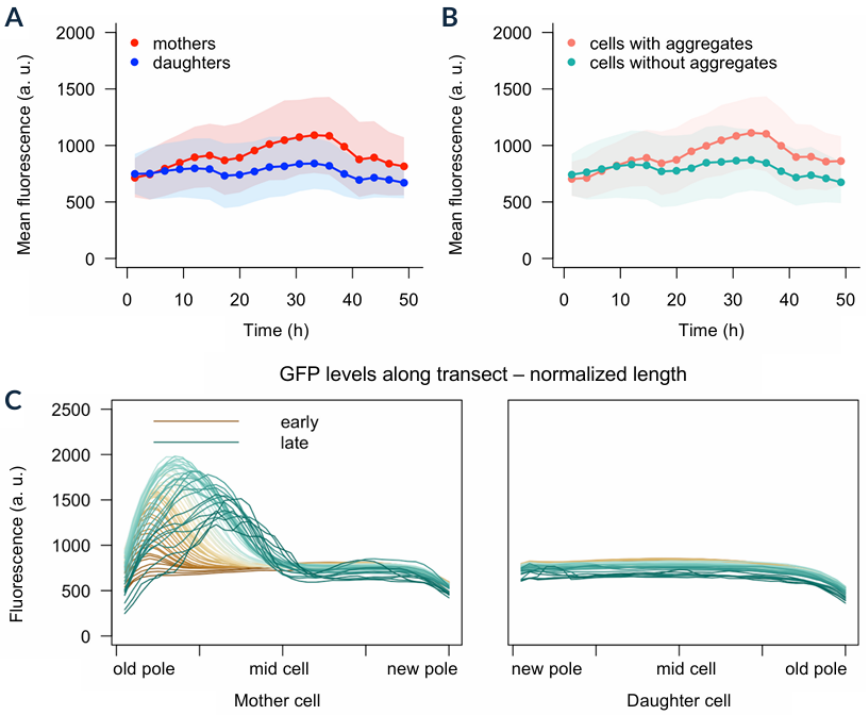

Fig. 2. Fluorescence increases over time in mother cells due to aggregates. (A) Mean fluorescence increases over time in mother cells but not in daughters. (B) When the population is divided according to the presence/absence of aggregates, they show a similar increase in mean fluorescence over time as (A), suggesting strong overlap of mother-cell and aggregate-bearing subgroups. Bins = mean ± SD. (C) Mean DnaK-msfGFP fluorescence profiles of mother (left) and daughter cells (right) from old to new pole. Each line represents the average transect for a given generation over a normalized cell length. The mother shows increased GFP levels, indicating protein aggregation, near the old pole.

Protein aggregates in mother cells increase in length over time

To further investigate whether mother cells accumulate misfolded proteins into aggregates as they age, we quantified DnaK fluorescence transects (Fig. 2C). For this, we traced the mean fluorescence profile along the length of each cell, from old to new pole, after division. The resulting data was used to detect localized fluorescence peaks (see Methods for details) and measure their diameter, intracellular position, and mean intensity. By plotting the mean transect for each generation (Fig. 2C), we observed increasingly large peaks associated with maternal old poles. The aggregates showed an average distance of 2.3 px from the old pole, which represents 4% of the mean length of a mother cell at beginning of a cell cycle (56.6 px). Since the average daughter transect showed homogeneous levels of intracellular fluorescence, the occurrence of aggregates is likely rare among these cells.

The differential inheritance of protein aggregates is supported by their presence after each division (Fig. 3A). The frequency of aggregate-free mother cells declined sharply after 10 h, indicating the formation and retention of aggregates with age, whereas most daughters were born without aggregates throughout the 48 h of observation. As suggested by the fluorescence profiles in Fig. 2C, maternal aggregates grew larger over time (generalized additive model (GAM), aggregate length in response to time; $F = 913$, $p < 0.001$; Fig. 3BC). This model, using a smooth function of time modified by inherited pole (mother / daughter), accounted for 45.7% of the deviance in observed aggregate length. A few daughters carried discernible aggregates, which were smaller in size. The size of aggregates found in daughter cells was hardly affected by maternal age (GAM, aggregate length in response to time; $F = 6.11$, $p < 0.001$). Together, these results corroborate that mother cells accumulate misfolded proteins in the form of aggregates as they age, with the retention of damaged proteins in their old poles leading to the asymmetric partitioning of misfolded components upon division.

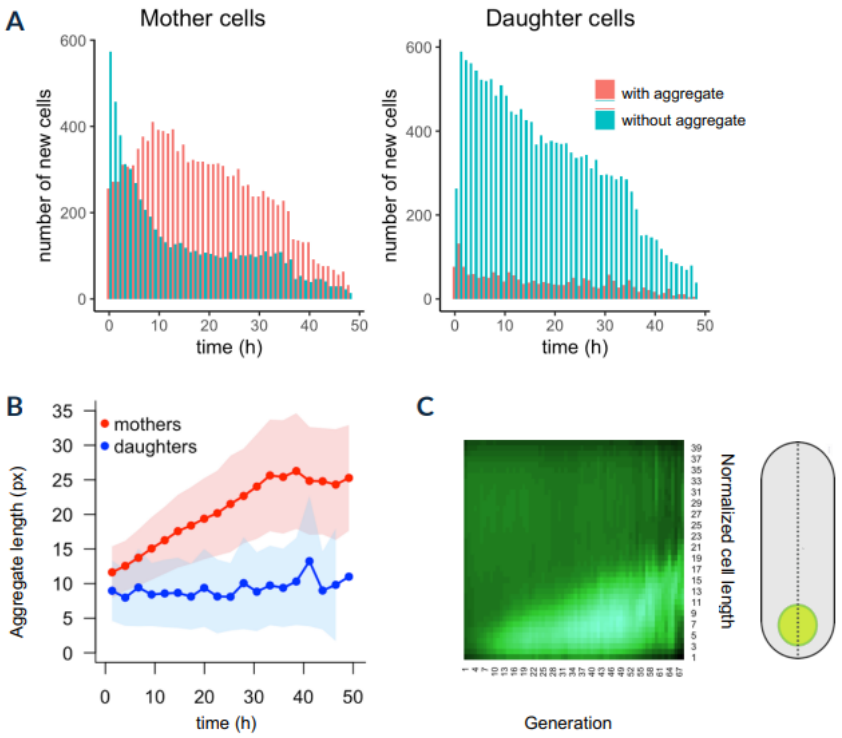

Fig. 3. Distribution and size of protein aggregates in mother and daughter cells. (A) Within a few hours, most mother cells harbored protein aggregates, contrasted by a consistently low proportion of daughter cells carrying them. This indicates that mothers retain aggregates at the old cell poles. Bars represent the number of cells per hour that emerge from a division. (B) Protein aggregates increase in size in mother cells over time, while no comparable increase is seen among the few daughters that carry aggregates. Bins = mean ± SD. (C) Heatmap showing expression and localization of DnaK-msfGFP in mother cells along the transect with progressing replicative age (in generations). Cell length was normalized, with 1 representing the old pole of the cell. For reference, to the right is a graphic representation of an aggregate-bearing cell showing the transect as a dotted line going from pole to pole.

Disperse damage is more harmful than protein aggregation

The sharp increase in aggregate size over time contrasts with the stability of bacterial elongation rates across generations, found in our results as well as in many previous studies (*9*, *28*, *33*). Whether through a toxic effect of harboring misfolded proteins or through the increased investment of resources into damage repair, it has been widely assumed that protein aggregation should correlate with slower growth (*8*, *11*). Past models have proposed that mother cells reach a state of growth stability once the intracellular damage load retained after each division becomes constant (*15*, *26*). However, our data

suggests that damage levels continue to climb long after mother cells have reached this state of equilibrium (Fig. 3B). We must therefore investigate whether the accumulation of misfolded proteins correlates with a physiological decline (*8*) or has no effect on growth (*27*).

Considering the whole population, the presence of a protein aggregate had a statistically significant, albeit small, effect on elongation rates (Fig. 4A): cells bearing an aggregate grew slightly more slowly (0.0156 ± 0.0039 min^{-1}) than aggregate-free cells (0.0162 ± 0.0049 min^{-1}). However, this difference did not factor the inheritance of old or new poles upon division. By repeating this analysis on split subpopulations of mother and daughter cells, we found that this trend was surprisingly reversed (Fig. 4B). Each subpopulation exhibited a slightly decreased elongation rate in aggregate-free cells, comparing to aggregate-bearing ones (F test, $F_{3,\ 35385} = 1086$, $p < 0.001$, $R^2 = 0.08$). Although the difference was marginal, this suggests that the simple presence of an aggregate does not imply slower growth, once we account for the underlying asymmetry between mothers and daughters.

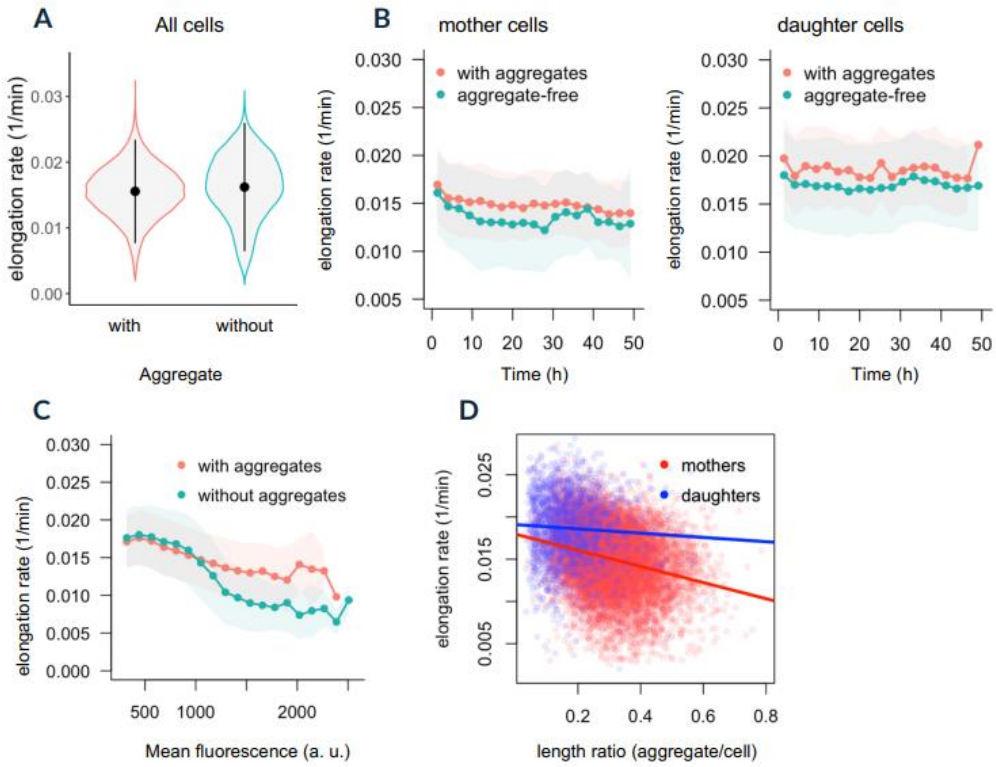

Fig. 4. Effect of protein aggregates on cell growth. Bins = mean ± SD. (A) When considering the population as a whole, elongation rates were negatively impacted by the presence of protein aggregates. (B) Splitting the sample into subpopulations of mothers and daughters, however, showed the opposite effect. Within subpopulations, aggregate-bearing cells had consistently greater elongation rates than aggregate-free cells. (C) Intracellular damage loads, as indicated by mean fluorescence, were negatively correlated with elongation rates. High damage concentrations (above 1,000 a.u.) led to a shaper growth decline in cells without aggregates, indicating that disperse misfolded proteins might be more harmful to the cell. (D) Scatterplot with regression lines showing that the relative size of protein aggregates is negatively correlated with cell growth.

This observation appears to stand in contrast with the progressive accumulation of damage we found among mother cells, and the correlation between the inheritance of old poles and slower elongation rates. Could it mean that protein aggregation has a protective effect against damage accumulation? To investigate this, we evaluated the mean fluorescence of all cells in the population.

Our time-lapse images suggested that, in some cases, growing cells with no discernible aggregates could nonetheless exhibit a high concentration of DnaK-msfGFP. In both mothers and daughters, a fraction of aggregate-free cells showed a mean fluorescence higher than 1,000 a.u., an intensity threshold associated with the formation of a polar aggregate in most other cases (Fig. 2C): fluorescence foci had an average intensity of 1,324.1 ± 537.7 a.u., with their peaks reaching 2,147.3 ± 1,078 a.u., whereas aggregate-free cells showed a mean fluorescence of 799 ± 277.8 a.u.. By plotting the mean fluorescence of aggregate-free and aggregate-bearing subpopulations against their elongation rates, we observed that a clear distinction emerges for higher DnaK concentrations (Fig. 4C). Although higher fluorescence corresponded to a slower growth in both cases, the effect of intracellular damage levels on elongation rates was modified by whether the cells had aggregates (GAM; $F = 284.3$, $p < 0.001$) or not ($F = 709.2$, $p < 0.001$), explaining 18% of the deviance in elongation rates.

These findings suggest that an increased damage load in the cell may be less disruptive to cellular growth when it is focused or aggregated near the cell pole, rather than dispersed throughout the entire cell — especially when its concentration reaches the levels usually found in protein aggregates. This raises an interesting perspective on bacterial asymmetry: so far, the asymmetric partitioning of damage has been considered advantageous in face of high damage accumulation rates, as it might allow for faster population growth than symmetric partitioning (*16*) and lead to differential stress survival (*15*, *25*). However, these past models considered that a given damage load would have the same effect on cellular growth whether dispersed or gathered in the pole. If damage aggregation decreases the cost of bearing this intracellular load, the very mechanism of asymmetry might provide a fitness advantage over symmetrically dividing cells, which face the increased cost of dispersed damage.

Cell aging is determined by the relative size of aggregates

Recent studies have shown that ribosomes (*21*) and newly synthesized proteins (*22*) are differentially inherited by the daughter cell, largely due to the exclusion of these components from maternal old poles by protein aggregates (*19*). Thus, the advantage of aggregate-bearing cells could derive from the confinement of damage and repair functions to a smaller area near the cell pole, leaving more free space for processes necessary for healthy cell functioning and growth. In other words, the defining feature affecting *E. coli* cell growth might be the amount of aggregate-free space in the cell. We tested this hypothesis by determining the fraction of the cell occupied by an aggregate (*i.e.* relative aggregate length) and using an ANCOVA to determine its effect on elongation rates as a function of cell pole inheritance. We found a negative effect of relative aggregate length on maternal elongation rates (F test, $F_{3, 13821} = 825.4$, $p < 0.001$, $R^2 = 0.152$), but the same was not observed in daughter cells. This suggests that protein aggregates drive a physiological decline in mother cells through the spatial competition with other cellular processes.

Morphological asymmetry buffers against physiological decline

A puzzling discrepancy still emerges from our results. The size of protein aggregates accumulating in maternal old poles increases over time, with harmful effects on cellular growth depending on the relative size of these damage loads. Nonetheless, elongation rates remain stable across generations. In a bacterium that divides with morphological symmetry, where the size of the mother remains constant, it is not possible to reconcile these observations. If, however, mother cells were to balance out the space that is lost because of aggregates proteins by growing longer, this might allow the cell to sustain the normal functioning of growth and protein synthesis.

To test this hypothesis, we evaluated the effects of protein aggregates on the length of mother cells at the start of each cell cycle. Fitting a generalized linear model (GLM), we found that cell length increased with replicative age (Fig. 5A), and this effect was modified by the presence of protein

aggregates: aggregate-bearing mothers showed a steeper increase in length across generations (GLM: df = 1, 18265, deviance = 308, 912, $p < 0.001$). Because daughter cells did not follow such a length increase, a morphological asymmetry between mothers and daughters emerged (Fig. 5B; GLM: df = 1, 17780, deviance = 45, 353, $p < 0.001$), increasing over time in the presence of aggregates. In fact, this asymmetry increased with the aggregate size (Fig. 5C; GLM: df = 1, 11857, deviance = 26, 221, $p < 0.001$), as mother cells grew longer with the accumulation of intracellular damage. Taken together, these results indicate that cell length is affected by the presence and size of protein aggregates accumulated in maternal old poles, resulting in the appearance of morphologically asymmetric cell divisions with age. This length increase has the potential to buffer mother cells against the harmful effect of protein aggregation, allowing elongation rates to remain constant.

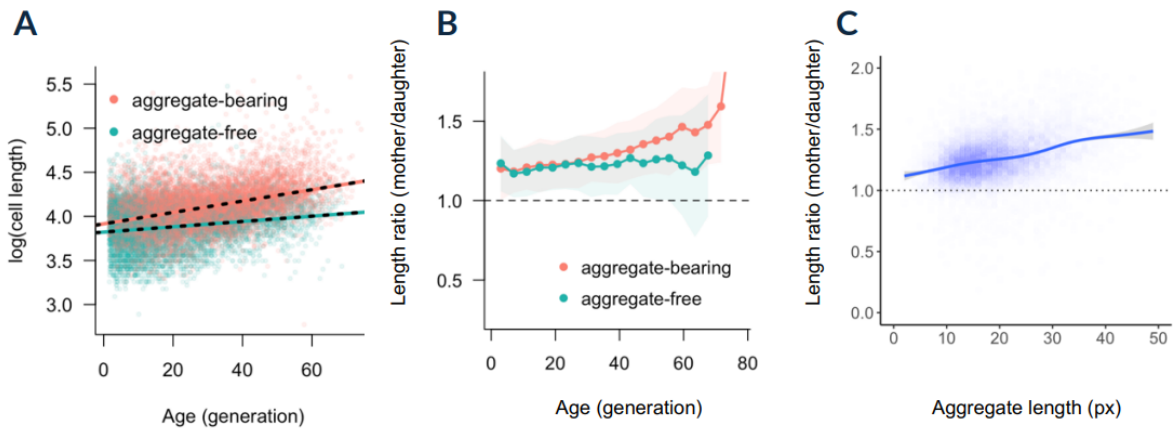

Fig. 5. Cell length increases in the presence of protein aggregates, driving length asymmetry. (A) With increasing replicative age, *E. coli* cells increased in length at birth (i.e., start of the cell cycle). The effect of age on length was greater when an aggregate was present. The scatterplot shows log transformed cell length by replicative age, with regression lines showing the interaction of age and presence of aggregates. (B) Morphological asymmetry appeared to be common, with mother cells emerging on average longer from division than daughters. This length asymmetry increased with age in aggregate-bearing cells. Bins = mean ± SD. (C) In divisions where the mother cell carried an aggregate, length asymmetry correlated positively with the size of the aggregate. Gray shading around the trend line represents the 95% confidence interval.

DISCUSSION

Bacteria age through the asymmetry between mother and daughter cells upon division, mirroring the separation between a soma and germline in complex organisms. This asymmetry is usually attributed to the uneven segregation of damaged proteins, but the impact of protein aggregation on the bacterial aging phenotype is clouded by conflicting results (*17*, *34*, *35*). The prevalent assumption was that protein aggregates accumulate in maternal old poles over time, leading to a physiological decline (*8*, *11*), but recent findings challenged this perspective by revealing a lack of correlation between aggregates and cell growth (*27*).

We addressed these contradictory findings, showing that mother cells gather misfolded proteins into polar aggregates that grow progressively larger over generations (Fig. 3). Although mother cells were likely to retain this damage upon division, the sole presence of an aggregate could not explain their lower elongation rates. Instead, we found that the main factor driving growth decline was the proportion of the intracellular space occupied by the aggregate (Fig. 4D). One possible explanation for this is the spatial competition between stored damage and the protein synthesis machinery. The intracellular organization of these components is influenced by the nucleoid (*36*), which holds

aggregates in the maternal old pole as they become larger (*12*). Protein aggregates themselves have been shown to hinder the diffusion of other intracellular components (*19*), displacing ribosomes (*21*) and newly synthesized proteins (*22*) towards the new pole. With increasing maternal age, the cell develops an intracellular gradient in gene expression, where the old pole has a lower contribution to the overall metabolism (*23*). Therefore, the relative size of a protein aggregate determines the physiological decline of the mother cell, as it competes with processes that are necessary for cell growth and functioning.

Nonetheless, an unexpected outcome emerged when we considered subpopulations of mother and daughter cells separately. Once the underlying age structure was taken into account, aggregate-bearing cells showed marginally faster elongation rates than aggregate-free cells (Fig. 4). This effect was more pronounced among cells with a high concentration of intracellular damage, suggesting that polar aggregates might be less detrimental to cellular functioning than similar levels of dispersed damage. This implies that protein aggregation can buffer an aging mother cell against a more severe physiological decline. For instance, if we assume that protein aggregates are spherical, damage accumulation should climb exponentially with age to explain the volume increase corresponding to diameters measured in Fig. 3B. As the observed growth decline was far less than exponential, it suggests a buffering of the aging process. This can be attributed to the gradual increase in maternal length as it accumulates larger aggregates (Fig. 5), which corresponds to previous reports that polar aggregates can lead to an off-center positioning of the FtsZ ring (*37*). The result is the emergence of a morphological asymmetry in *E. coli* division as the mother cell ages, mitigating the spatial competition between damaged proteins and other cellular components.

Protein aggregation is a well-observed feature of the aging phenotype, and previous research has shown that it can come with fitness advantages — one being asymmetrical segregation of damage during cell division, ensuring rejuvenated, immortal lineages within the population (*14*, *26*). The separation of damaged components from other cellular processes may not only benefit the offspring, but also allow the aging cell to sustain stable growth rates. As mother cells accumulate misfolded proteins in the form of polar-localized aggregates, they compensate for the lost intracellular space by increasing in length. Since this gradual elongation occurs through asymmetric fission, it is justified to assume that these cells continue to divide according to the "adder" model (*38*), growing by a constant length between divisions. This would allow aging cells to maintain a state of growth stability over generations (*9*, *28*, *33*), showing constant elongation rates despite the continuous accumulation of intracellular damage. For *E. coli*, this could mean that aging may not present as a steady growth decline but rather as a prolonged period of stable growth accompanied by focused damage accumulation, which eventually results in rapid decline and death when damage amounts have reached a lethal level. The existence of such mortality threshold has been suggested by mathematical models (*15*, *39*) and even estimated from experimental doubling times (*26*), but its direct quantification remains elusive.

Our findings provide a framework through which protein aggregation operates in bacterial lineages. Increasing damage loads accumulate in mother cells, but their detrimental effects can be buffered by a corresponding increase in length that allows for stable growth. These results, however, do not explain all mechanisms of bacterial aging. An aggregate-free mother cell still grows more slowly than its daughter, and an aggregate-bearing mother has lower elongation rates despite being buffered by a length increase. It is possible that mother cells show decreased growth not only due to harboring more damage, which they can compensate through increased length, but also due to the repair investment required to prevent the growth of protein aggregates from outpacing the lengthening of the cell. In addition, further aging mechanisms not linked to the accumulation of misfolded proteins might contribute to maternal aging, which might not be surprising given the known complexity of the aging

process even in simple unicellular organisms. Studies performed on *Caulobacter crescentus*, for example, suggest that bacteria might display other forms of aging even when the segregation of protein aggregates is symmetric (*40*). By demonstrating how apparently contradictory findings from past studies can coexist in bacterial aging, we provide insights for future studies that may continue to explore the various mechanisms of protein misfolding, aggregation, and repair to investigate the fundamental mechanisms of cellular aging.

MATERIALS AND METHODS

Bacterial strains and growth conditions

Escherichia coli strains MG1655 Δ*lacY dnaK-msfGFP* and MG1655 Δ*lacY* (wild-type) were developed at KU Leuven, Department of Microbial and Molecular Systems, for a previous study (*27*). *E. coli* MG1655 Δ*lacY dnaK-msfGFP* expresses a DnaK-msfGFP (monomeric superfolder GFP) fusion protein, which allows for the quantification of aggregate formation. Bacterial stocks were streaked into fresh LB plates, and a single colony was inoculated into 5 ml M9 minimal medium (1x M9 salts, 2 mM $MgSO_4$, 0.1 mM $CaCl_2$) supplemented with 0.4% glucose and 0.2% casamino acids, where it was grown overnight at 37° C with agitation. Before each experiment, 150 µl of the overnight culture was diluted into 15 ml of fresh medium and grown for 2 h at 37°C. For inoculation into microfluidic devices, the medium was supplemented with 1 µg/ml Propidium Iodide (PI) and 0.075% Tween20 (Sigma-Aldrich). PI facilitates the detection of cell lysis by intercalating with nucleic acids, and Tween20 was used to prevent cell adhesion inside the device. Throughout the microfluidics experiments temperatures were kept constant at 37°C.

Microfluidic device design and fabrication

The mother machine (*33*) is a microfluidic design that allows for the capture of individual bacterial cells inside narrow growth wells, while being fed fresh culture medium provided by wide flow channels. This allows for the capture of time-lapse images of individual cells growing in exponential phase over several generations. Cells at the closed end of the wells are considered “mothers” because they inherit the old pole in every division. Their new pole siblings, which get washed out of the well into the flow channels over time, are referred to as daughters. Our microfluidic design contained four parallel flow channels (1 cm x 80 µm x 10 µm) with inlet openings on one side and outlets on the other. At these inlets and outlets, metal connectors were connected to Tygon tubing (ND 100-80, Saint-Gobain, Darwin Microfluidics) to feed M9 media into the device and remove cells that had been washed out of the wells. Each flow channel contains 1,000 growth wells (25 x 0.8 x 1.2 µm) that are long enough for mothers not to get washed out too easily, while being short and wide enough for sufficient growth medium to reach mother cells.

We fabricated chips by pouring Sylgard 184 polydimethylsiloxane (PDMS, Dow Corning, USA) into epoxy molds that had been cast from original laser-etched wafers. After pouring, PDMS was degassed to eliminate bubbles introduced during mixing, then cured at 80°C for 60 min. After careful demolding and cropping of the chips, we created inlet and outlet ports at the ends of the flow channels using a 0.5 mm biopsy puncher (Shoney Scientific). Subsequently, chips and ports were washed with ethanol and rinsed with distilled water prior to bonding to 24 x 40 mm coverslips using a plasma cleaner. Bonded chips were immediately placed on a heating plate at 80°C for 2 min, and incubated at 60°C overnight. One hour before cell loading, chips were plasma-activated and flushed with 20% polyethylene glycol (PEG) to aid media flow and prevent cell attachment.

Cell loading and experimental conditions

Exponential bacterial cultures were centrifuged at 4,000 rpm for 10 min, and the resulting pellet was resuspended into 200 µl of M9 medium. The suspension was injected through the outlet port of each flow channel, followed by the centrifugation of the chip at 1,500 rpm for 8 min to push bacteria into the growth wells. After inspecting the chip under the microscope to ensure that loading was successful, it was connected to inlet tubing running through a peristaltic pump (Ole Dich, Denmark) to generate a constant flow of 200 µl/h. At the outlet ports of the loaded chip, another set of tubing was connected to a waste container to collect the outflow. The chip was then placed in the microscope's temperature-controlled incubation chamber (Pecon TempController 2000-1, set to 37°C) for the duration of each experiment.

Microscopy and image acquisition

Time-lapse images were captured with a DS-Qi2 camera connected to an inverted microscope (Nikon Eclipse Ti2) equipped with a motorized stage and Perfect Focus System (PFS). Using a 100x oil objective and the NIS Elements software, once a chip was mounted in the microscope, we selected 12 fields for automated image capture in 2 min intervals. GFP and RFP fluorescence imaging (400 ms exposure and 8% intensity) was set to 10 min intervals to reduce phototoxic stress while providing sufficient data. Two separate replicates were performed for each strain.

Image processing

After the experiments, images were first adjusted on ImageJ for chromatic shift correction and background subtraction of fluorescence images (rolling ball radius = 12 px). The tool Deep Learning for Time-lapse Analysis (DeLTA) (*41*) was used for automated image processing, which was previously trained on data from our experimental setup. This procedure was performed on the High-Performance Computing center at FU Berlin (*42*). Phase contrast images were used to perform cell segmentation and tracking. The DeLTA output was then converted into R data serialization (RDS) files and visually inspected for quality control. The data for each bacterial lineage was run through a custom R script (version 2023.12.1+402) to correct obvious tracking errors, remove empty or only partially captured wells, and crop wells where severe tracking and segmentation errors occurred. Where necessary, further manual corrections were performed with the same custom R script.

Quantification of bacterial growth

Elongation rates were used as a measure of cellular growth and fitness, because the rate at which the cell increases in length is crucial for its ability to double its length and divide. To measure elongation rates, each cell was followed from its "birth" until the point where it divided again, and the division interval was determined. Cell length was measured along the cell cycle. Based on these measurements and considering that *E. coli* cell growth is exponential in nature, elongation rates were calculated as the exponential fit of the length increase of each cell over time. As mother and daughter cells originating from the same division were paired in the data, we were also able to determine morphological asymmetry by using length measurements after division to calculate the ratio of mother cell birth length to daughter cell birth length.

Quantification of dispersed fluorescence and protein aggregates

To determine intracellular damage and protein aggregates, the first fluorescence image of each cell cycle was measured in terms of the brightness of each pixel within the area of the cell. The GFP signal intensity was measured in an arbitrary unit, as fluorescence measurements depend on the microscope and its settings –the same settings were used in all experimental runs, prioritizing resolution

at the bright end of the spectrum as we were interested in the areas of the cells with the most fluorescence. To determine the mean intensity of GFP fluorescence and thereby assess the relative amount of DnaK-indicated damage load per cell, an average value over all pixels in the cell was calculated. The intensity peak for each cell was measured as the GFP signal intensity in the brightest pixel of the cell.

From the DeLTA output, we obtained a pixel-by-pixel fluorescence profile along a transect running through the center of each cell, from the old pole to the new pole. In a cell with diffused fluorescence, transect measurements were relatively uniform. However, many cells displayed extreme spikes in fluorescence near the old poles, which could be detected as outliers in the transect data. By locating these outliers using the function findpeaks() in R, areas with a very high density of DnaK-msfGFP, representing aggregates, could be detected and their absolute length, distance to the old pole, intensity peak and mean fluorescence were determined with a custom R script. The ratio of aggregate length to cell length was calculated to gain information about the proportion of the cell which was taken by the aggregate. For visualization of the mean transect measurements over generations, generations with fewer than 10 cells were removed.

Statistical analysis

All statistical analyses were performed in R (version 2023.12.1+402). Included in the analysis were mother cells as well as their immediate new pole offspring (daughters). These pairs of old and new pole cells born in the same division formed a set of paired data points, each of them observed from its birth until its next division. Any cells that did not complete their life cycle and whose next division was therefore not captured were excluded from the analysis. In the same vein, cells that started their cell cycle before image capture began were also excluded. Mother cell age was determined both in the sense of replicative age (counted in generations) and chronological age, the latter with a resolution of 2 min, as this was the imaging interval. Generation and time count started with the start of imaging. For parametric testing, data was log-transformed as necessary, and linear models were checked for normality and homoskedasticity; where model assumptions were violated, generalized linear models or generalized additive models were fitted instead. Data was standardized or normalized only in service of plotting, but not for statistical testing. In visual representations, plots with binned data show the mean ± standard deviation (SD), leaving out bins which comprised fewer than 10 data points.

ACKNOWLEDGEMENTS

We thank L. Stäcker and M. Lajine for experimental support. The authors would like to thank the HPC Service of FUB-IT, Freie Universität Berlin, for computing time. AN was funded by the German Research Foundation (grant 430174701), MT by the Marie Skłodowska-Curie Actions' European Postdoctoral Fellowship (grant 101069035), UKS by the Heisenberg Programme of the German Research Foundation (grant 430170797), and AMP was funded by the Humboldt Research Fellowship (Alexander von Humboldt Foundation, Germany).

REFERENCES

1. C. López-Otín, M. A. Blasco, L. Partridge, M. Serrano, G. Kroemer, The hallmarks of aging. *Cell*. **153**, 1194–1217 (2013).

2. M. R. Rose, *Evolutionary Biology of Aging* (Oxford University Press, New York, 1991).

3. T. B. L. Kirkwood, Evolution of ageing. **270**, 301–304 (1977).

4. M. Coelho, S. J. Lade, S. Alberti, T. Gross, I. M. Tolic, Fusion of Protein Aggregates Facilitates Asymmetric Damage Segregation. *PLoS Biol.* **12**, e1001886 (2014).

5. S. R. Laney, R. J. Olson, H. M. Sosik, Diatoms favor their younger daughters. *Limnol. Oceanogr*. **57**, 1572–1578 (2012).

6. M. Ackermann, S. C. Stearns, U. Jenal, Senescence in a Bacterium with Asymmetric Division. *Science (80-.).* **300**, 1920 (2003).

7. E. J. Stewart, R. Madden, G. Paul, F. Taddei, Aging and death in an organism that reproduces by morphologically symmetric division. *PLoS Biol.* **3**, e45 (2005).

8. A. B. Lindner, R. Madden, A. Demarez, E. J. Stewart, F. Taddei, Asymmetric segregation of protein aggregates is associated with cellular aging and rejuvenation. *Proc. Natl. Acad. Sci. U. S. A.* **105**, 3076–81 (2008).

9. A. M. Proenca, C. U. Rang, C. Buetz, C. Shi, L. Chao, Age structure landscapes emerge from the equilibrium between aging and rejuvenation in bacterial populations. *Nat. Commun.* **9**, 3722 (2018).

10. U. K. Steiner, A. Lenart, M. Ni, P. Chen, X. Song, F. Taddei, J. W. Vaupel, A. B. Lindner, Two stochastic processes shape diverse senescence patterns in a single-cell organism. *Evolution (N. Y).* **73**, 847–857 (2019).

11. J. Winkler, A. Seybert, L. König, S. Pruggnaller, U. Haselmann, V. Sourjik, M. Weiss, A. S. Frangakis, A. Mogk, B. Bukau, Quantitative and spatio-temporal features of protein aggregation in Escherichia coli and consequences on protein quality control and cellular ageing. *EMBO J.* **29**, 910–23 (2010).

12. A. S. Coquel, J. P. Jacob, M. Primet, A. Demarez, M. Dimiccoli, T. Julou, L. Moisan, A. B. Lindner, H. Berry, Localization of Protein Aggregation in Escherichia coli Is Governed by Diffusion and Nucleoid Macromolecular Crowding Effect. *PLoS Comput. Biol.* **9** (2013), doi:10.1371/journal.pcbi.1003038.

13. L. Partridge, N. H. Barton, Optimally, mutation and the evolution of ageing. *Nature*. **362**, 305–311 (1993).

14. M. Ackermann, L. Chao, C. T. Bergstrom, M. Doebeli, On the evolutionary origin of aging. *Aging Cell*. **6**, 235–44 (2007).

15. L. Chao, A model for damage load and its implications for the evolution of bacterial aging. *PLoS Genet.* **6**, e1001076 (2010).

16. S. N. Evans, D. Steinsaltz, Damage segregation at fissioning may increase growth rates: A superprocess model. *Theor. Popul. Biol.* **71**, 473–490 (2007).

17. F. D. Schramm, K. Schroeder, K. Jonas, Protein aggregation in bacteria. *FEMS Microbiol. Rev.* **fuz026**, 54–72 (2020).

18. M. S. Hipp, P. Kasturi, F. U. Hartl, The proteostasis network and its decline in ageing. *Nat. Rev. Mol. Cell Biol.* **20**, 421–435 (2019).

19. D. Linnik, I. Maslov, C. M. Punter, B. Poolman, Dynamic structure of E. coli cytoplasm: supramolecular complexes and cell aging impact spatial distribution and mobility of proteins. *Commun. Biol.* **7** (2024), doi:10.1038/s42003-024-06216-3.

20. Y. Xiang, I. V. Surovtsev, Y. Chang, S. K. Govers, B. R. Parry, J. Liu, C. Jacobs-Wagner, Interconnecting solvent quality, transcription, and chromosome folding in Escherichia coli. *Cell*. **184**, 3626-3642.e14 (2021).

21. L. Chao, C. K. Chen, C. Shi, C. U. Rang, Spatial and temporal distribution of ribosomes in single cells reveals aging differences between old and new daughters of Escherichia coli. *Elife*. **12**, RP89543 (2023).

22. C. Shi, L. Chao, A. M. Proenca, A. Qiu, J. Chao, C. U. Rang, Allocation of gene products to daughter cells is determined by the age of the mother in single Escherichia coli cells. *Proc. R. Soc. B.* **287**, 20200569 (2020).

23. A. M. Proenca, M. Tuğrul, A. Nath, U. K. Steiner, Declining old pole physiology gradually enhances gene expression asymmetry in bacteria. *bioRxiv* (2023), doi:10.1101/2023.08.07.552301.

24. J. Tyedmers, A. Mogk, B. Bukau, Cellular strategies for controlling protein aggregation. *Nat. Rev. Mol. Cell Biol.* **11**, 777–788 (2010).

25. L. Chao, C. U. Rang, A. M. Proenca, J. U. Chao, Asymmetrical Damage Partitioning in Bacteria: A Model for the Evolution of Stochasticity, Determinism, and Genetic Assimilation. *PLoS Comput. Biol.* **12**, e1004700 (2016).

26. A. M. Proenca, C. U. Rang, A. Qiu, C. Shi, L. Chao, Cell aging preserves cellular immortality in the presence of lethal levels of damage. *PLOS Biol.* **17**, e3000266 (2019).

27. S. K. Govers, J. Mortier, A. Adam, A. Aertsen, Protein aggregates encode epigenetic memory of stressful encounters in individual Escherichia coli cells. *PLOS Biol.* **16**, e2003853 (2018).

28. U. Łapińska, G. Glover, P. Capilla-Lasheras, A. J. Young, S. Pagliara, Bacterial ageing in the absence of external stressors. *Philos. Trans. R. Soc. B Biol. Sci.* **374** (2019), doi:10.1098/rstb.2018.0442.

29. L. Dewachter, C. Bollen, D. Wilmaerts, E. Louwagie, P. Herpels, P. Matthay, L. Khodaparast, L. Khodaparast, F. Rousseau, J. Schymkowitz, J. Michiels, The dynamic transition of persistence toward the Viable but Nonculturable state during stationary phase is driven by protein aggregation. *MBio*. **12**, e00703-21 (2021).

30. M. Lemoine, The Evolution of the Hallmarks of Aging. *Front. Genet.* **12** (2021), doi:10.3389/fgene.2021.693071.

31. C. Hu, J. Yang, Z. Qi, H. Wu, B. Wang, F. Zou, H. Mei, J. Liu, W. Wang, Q. Liu, Heat shock proteins: Biological functions, pathological roles, and therapeutic opportunities. *MedComm*. **3**, e161

(2022).
32. P. Wang, L. Robert, J. Pelletier, W. L. Dang, F. Taddei, A. Wright, S. Jun, Robust growth of Escherichia coli. *Curr. Biol.* **20**, 1099–103 (2010).
33. U. I. Baig, B. J. Bhadbhade, D. Mariyam, M. G. Watve, Protein aggregation in E. coli : short term and long term effects of nutrient density. *PLoS One*. **9**, e107445 (2014).
34. U. K. Steiner, Senescence in Bacteria and Its Underlying Mechanisms. *Front. Cell Dev. Biol.* **9**, 1–15 (2021).
35. Q. Chai, B. Singh, K. Peisker, N. Metzendorf, X. Ge, S. Dasgupta, S. Sanyal, Organization of ribosomes and nucleoids in Escherichia coli cells during growth and in quiescence. *J. Biol. Chem.* **289**, 11342–11352 (2014).
36. J. Mortier, S. K. Govers, A. Cambré, R. Van Eyken, J. Verheul, T. den Blaauwen, A. Aertsen, Protein aggregates act as a deterministic disruptor during bacterial cell size homeostasis. *Cell. Mol. Life Sci.* **80**, 1–13 (2023).
37. S. Taheri-Araghi, S. Bradde, J. T. Sauls, N. S. Hill, P. A. Levin, J. Paulsson, M. Vergassola, S. Jun, Cell-Size Control and Homeostasis in Bacteria. *Curr. Biol.* **25**, 385–391 (2015).
38. M. Tuğrul, U. K. Steiner, Demographic Consequences of Damage Dynamics in Single-Cell Ageing. *bioRxiv* (2023), doi:10.1101/2023.05.23.538602.
39. J. B. Lugagne, H. Lin, M. J. Dunlop, DeLTA: Automated cell segmentation, tracking, and lineage reconstruction using deep learning. *PLoS Comput. Biol.* **16**, 1–18 (2020).
40. L. Bennett, B. Melchers, B. Proppe, “CURTA A General-purpose High-Performance Computer at ZEDAT, Freie Universität Berlin” (2020), , doi:http://dx.doi.org/10.17169/refubium-26754.